Scientific Research Publishing

Open Journal of Fluid Dynamics, 2024, 14, 123-146
https://www.scirp.org/journal/ojfd
ISSN Online: 2165-3860
ISSN Print: 2165-3852

Influence of Temperature-Dependent Thermophysical Properties of TiO_2-SiO_2-ZnO-Fe_2O_3/PAO Tetra-Hybrid Nanofluid along a Vertical Porous Surface with Suction

Philip Iyiola Farayola[1], Lateefat Olanike Aselebe[2*], Kafilat Adebimpe Salaudeen[1], Saheed Dolapo Ogundiran[3], Tajudeen Motunrayo Asiru[1]

[1]Department of Mathematics and Computing Science Education, Emmanuel Alayande University of Education, Oyo, Nigeria
[2]Department of General Studies, Federal School of Surveying, Oyo, Nigeria
[3]Department of Pure and Applied Mathematics, Ladoke Akintola University of Technology, Ogbomoso, Nigeria
Email: farayola_pi@yahoo.com, *aselebelateefatolanike08@gmail.com, salaudeenka@gmail.com, ogundiransaheed81@gmail.com, tunra2014@yahoo.com

How to cite this paper: Farayola, P.I., Aselebe, L.O., Salaudeen, K.A., Ogundiran, S.D. and Asiru, T.M. (2024) Influence of Temperature-Dependent Thermophysical Properties of TiO_2-SiO_2-ZnO-Fe_2O_3/PAO Tetra-Hybrid Nanofluid along a Vertical Porous Surface with Suction. *Open Journal of Fluid Dynamics*, **14**, 123-146.
https://doi.org/10.4236/ojfd.2024.143006

Received: April 15, 2024
Accepted: August 5, 2024
Published: August 8, 2024

Abstract

The significance of the thermophysical properties of Tetra hybrid nanofluid in enhancing heat transmission in various applications like heat exchangers, automobiles, and solar storage cannot be overstated. These features can be tampered with when nanoparticles are been introduced into the base fluid to produce an improved heat carrier fluid for the system. This study investigates the impact of temperature-dependent properties on the movement of TiO_2-SiO_2-ZnO-Fe_2O_3/PAO Tetra hybrid nanofluid along a vertical porous surface with suction. The system of governing Partial Differential Equations (PDEs) was formulated and transformed into the system of coupled nonlinear third-order Ordinary Differential Equations (ODEs) by similarity techniques. The resulting ODEs were solved numerically using the shooting method and fourth order Runge-Kutta method with the aid of Maple 18.0 software. Using numerical and statistical methods, the study analyzes velocity, temperature profiles, skin friction coefficient, and Nusselt number. It was found that as the variable thermal conductivity parameter upsurges both the skin friction coefficient and Nusselt number intensify at the rate of **0.011697519** and **8.043581616** respectively. This study underscores the vital role of Tetra hybrid nanofluid's thermophysical properties in improving heat transmission for diverse applications. By manipulating nanoparticles within the base fluid, the heat carrier fluid's efficiency can be enhanced, critical for industries like automotive and

renewable energy. These insights inform the design of more efficient heat exchange systems, advancing sustainability and performance in real-world scenarios.

Keywords

Tetra Hybrid Nanofluid, Shooting Technique, Numerical Method, Skin Friction, Nusselt Number, Thermophysical Properties

1. Introduction

The investigation of nanofluids and their thermal physical characteristics has gained the attention of researchers in recent times due to their ability to enhance and improve the rate of heat transfer in manufacturing, heat exchangers, automobiles, and solar energy systems. Heat moves from the region of high temperature to the region of low temperature in a system with the aid of heat carrier fluid. The traditional heat carrier fluids are water, oils, salt water, and ethyl glycol. However, these fluids meant to carrier heat possess low thermal conductivity [1]. The implication of this challenge is the short life span of the system due to overheating or destruction of the engines. Researchers and scientists have solved this issue by introducing extremely tiny particles called nanoparticles (NPs) like metals (Copper (Cu), Aluminum (Al), Silver (Ag)), metal oxides (Copper oxide, (CuO), Aluminum oxide (Al_2O_3), carbon nanotubes (Diamond, Graphene), organic materials (Titanium oxide (TiO_2), Silicon oxide (SiO_2), Iron oxide (Fe_2O_3)) that have high thermal conductivity into the convectional base fluid to improve its rate of heat transfer. The resulting fluid is called Nanofluid (NF) [2]. This upgraded heat carrier fluid serves better as a lubricant, coolant agent and prolongation of the systems in industries, automobiles, heat exchangers and more. Researchers like [3]-[6] have thoroughly studied NF.

Nanofluid, as it is full of potential, its steadiness depends on the size of the particles, thermophysical properties, temperature, and other dimensionless parameters [3]. The thermophysical properties of NF need to be focused on to meet the worldwide demand for smaller sizes and yet highly effective heat exchanger systems in the industry [6]. Because the addition of appropriate NPs into the base fluid usually increases its thermophysical properties. However, the focus of many researchers is thermal conductivity because it is the main target of any improved heat carrier fluids [7]. The study of thermal conductivity is widely done by [8]-[14]. As mentioned earlier, other properties along with thermal conductivity also increased as NPs are included in the traditional heat carrier fluids. For example, viscosity is a feature of fluid that causes a restriction on the fluid to move easily and quickly to the vital parts of the system [15]. It is important to focus on this characteristic as it can damage the engine entirely due to friction and wear [16]. A series of research has been made on the viscosity of nanofluid in aiding the improvement of heat transfer efficiency [17]-[22] and

many more.

Another crucial property of improved fluid is density. It is being affected by the inclusion of the NPs by upsurging the mass per volume of fluid [23]. This property is as important as other properties because changes in mass per volume of fluid influence so many aspects of fluid compartments within the engines and machines [24] [25]. It could affect buoyancy which is the measure of upward forces exerted by the fluid on an object immersed in a fluid which can influence the stability of the systems [26].

Similarly, the compactness of the heat exchanger systems can be influenced by the specific heat capacity of the fluid used within them [27]. This is another characteristic of fluid that is meant to be carefully considered in the process of improving the rate of heat transfer of the improved fluid [28]. Changes in specific heat capacity can alter the overall thermal performance of the fluid. This characteristic of NF can influence the effectiveness of heat transfer in the system, its changes due to the inclusion of NPs can affect the heat exchanger unit, sizes, and designs of the system [29]. Thus, nanofluids with boosted thermophysical features are seen as a significant potential resolution to augmentation of heat transmission performance in heat exchanger systems [6].

The issues of sedimentation, aggregation, and instability of nanofluid led to the existence of Hybrid Nanofluid (HNF). This fluid exhibits outstanding heat transfer improvement than NF [30]. It involves the dispersion of more than one NP in the base fluid, and it has gained the attention of researchers [31]. The challenge of hybrid nanofluid is the high viscosity causing an increased drag leading to more power for fluid movement leading to less effective and efficient systems [32]. Researchers have done numerous works on Hybrid nanofluids [33] [34] and Trihybrid Nanofluids [35]-[39].

Tetra-hybrid nanofluid which comprises four different NPs being introduced into the base fluid to improve the rate of heat transfer of heat carrier fluid is another interesting fluid [40] [41] [42]. It can be broadly used in heat exchangers, automobiles, and biotechnology [43] [44]. In literature, the tetra-hybrid nanofluid started gaining popularity among researchers because of its outstanding improvement in the realm of transmission of heat from the region with higher temperature to the region with lower temperature.

Polyalphaolefin (PAO) is widely recognized for its outstanding thermal stability and is extensively used as a synthetic oil in industrial applications [45]. It does not contain nitrogen components and possesses high viscosity which makes it excellently applicable where thick and durable lubricant oil is required. The incorporation of NPs such as TiO_2, SiO_2, ZnO and Fe_2O_3 has shown a potential to enhance engine efficiency. [46]-[49] concluded that the rate of heat transfer of fluid is enhanced with the addition of hybrid nanoparticles in the base fluid. However, careful formulation is crucial to prevent issues related to excessive viscosity that could impede lubricant movement and potentially damage the engine. Therefore, achieving proper thermophysical properties in nano lubricants

across a range of temperatures is essential for optimal performance.

While previous research has extensively studied nanofluids and hybrid nanofluids, the specific composition and thermal behaviour of Tetra hybrid nanofluids remain relatively unexplored. This research therefore aims to bridge the gap by numerically investigating the temperature-dependent thermophysical properties of TiO_2-SiO_2-ZnO-Fe_2O_3/PAO tetra hybrid nanofluid in the presence of suction along a vertical porous surface. Understanding these properties is crucial for optimizing heat transfer processes in various applications, including heat exchangers, automobiles, and solar energy systems. The objectives of this study are twofold: 1) to determine the effects of Tetra hybrid nanofluid's changeable temperature-dependent thermophysical parameters, including thermal conductivity, viscosity, density, and specific heat capacity, on the system's heat transmission rate, and 2) to analyze the rate of change of dependent variables—skin friction and Nusselt number—in relation to the independent variables (thermophysical parameters). By systematically examining these aspects, the research seeks to provide valuable insights into the behaviour and performance of characteristics of Tetra hybrid nanofluid, thus contributing to the advancement of nanofluid technology.

2. Mathematical Model Formulation

A two-dimensional steady incompressible flow of viscous and dielectric TiO_2-SiO_2-ZnO-Fe_2O_3 Tetra hybrid nanofluid moving through a porous vertical surface with suction, variable thermal conductivity, variable density, variable viscosity parameter, and variable specific heat capacity of tetra hybrid nanofluid was considered. The x-axis and y-axis are taken along the direction of the plate and normal respectively as shown in **Figure 1**. The left surface of the plate is heated by convection from a hot temperature, T_w^* which provides a heat transmission coefficient h_w^* while a flow of TiO_2-SiO_2-ZnO-Fe_2O_3/PAO tetra hybrid nanofluid at the free stream temperature T_∞^* moves along the right surface of the plate with a uniform free stream velocity U_∞^*. Equations (1)-(3) are continuity, momentum, and energy equations respectively.

$$\frac{\partial u^*}{\partial x^*}+\frac{\partial v^*}{\partial x^*}=0 \tag{1}$$

$$u^*\frac{\partial u^*}{\partial x^*}+v^*\frac{\partial u^*}{\partial y^*}=\frac{\partial}{\partial y^*}\left[\frac{\mu_{TetraNF}\left(T^*\right)}{\rho_{TetraNF}\left(T^*\right)}\frac{\partial u^*}{\partial y^*}\right]-\frac{\mu_{TetraNF}\left(T^*\right)}{\rho_{TetraNF}\left(T^*\right)\bar{k}}u^*+g\beta_{TetraNF}\left(T^*-T_\infty^*\right) \tag{2}$$

$$u^*\frac{\partial T^*}{\partial x^*}+v^*\frac{\partial T^*}{\partial y^*}=\frac{\partial}{\partial y^*}\left[\frac{K_{TetraNF}\left(T^*\right)}{\left(\rho C_p\right)_{TetraNF}\left(T^*\right)}\frac{\partial T^*}{\partial y^*}\right]+\frac{\mu_{TetraNF}\left(T^*\right)}{\left(\rho C_p\right)_{TetraNF}\left(T^*\right)}\left(\frac{\partial u^*}{\partial y^*}\right)^2 \tag{3}$$

On the right surface of the plate, the boundary condition is as follows:

$$u^*\left(x^*,0\right)=0, v^*\left(x^*,0\right)=-v_w^*, -k\frac{\partial T^*}{\partial y^*}\left(x^*,0\right)=h_w^*\left[T_w^*-T^*\left(x^*,0\right)\right] \quad \text{at} \quad y^*=0 \tag{4}$$

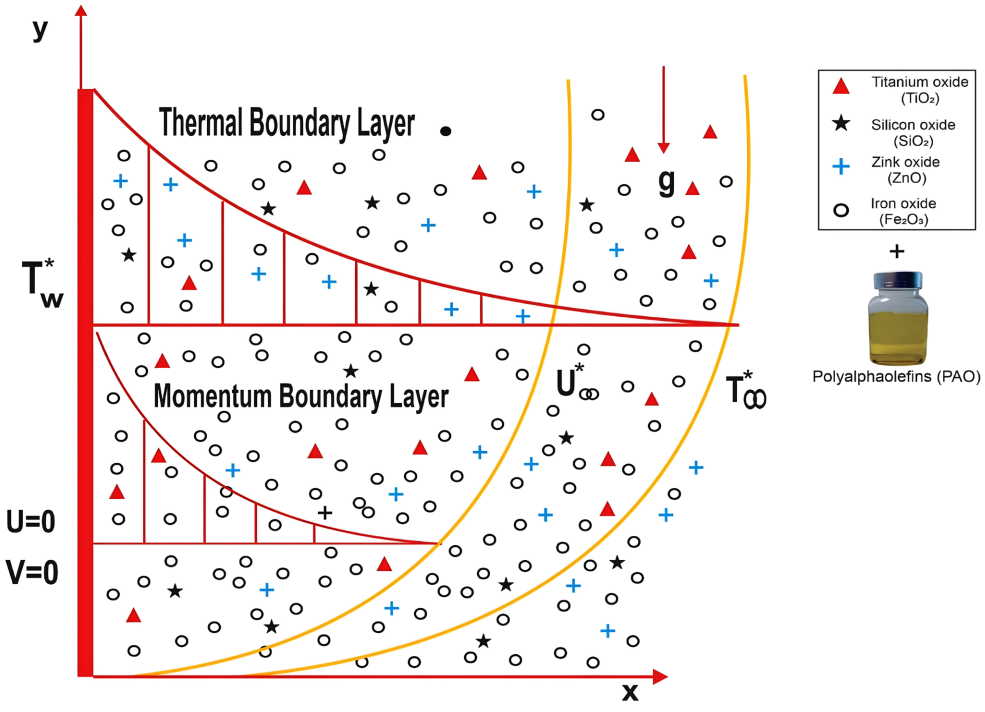

Figure 1. Geometry of the flow.

At the surface of the porous vertical plate, fluid temperature and velocity are specified, while suction influences fluid flow.

At the far right of the surface of the plate, the boundary condition of Tetra-PAO nanofluid is:

$$u^*\left(x^*,\infty\right)\to U_\infty^*, T^*\left(x^*,\infty\right)\to T_\infty^* \quad \text{at} \quad y^*\to\infty \tag{5}$$

At the far right of the plate, the fluid temperature remains constant, and a no-slip boundary condition is enforced for fluid velocity (Table 1).

Table 1. The shapes of the four nanoparticles.

Nanoparticles	Titanium oxide, (TiO_2)	Silicon oxide (SiO_2)	Zinc oxide (ZnO)	Iron oxide (Fe_2O_3)
Shapes		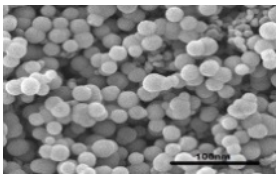		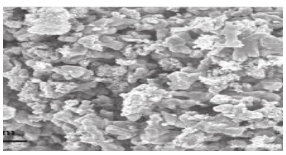

3. The Thermophysical Properties of Tetra Hybrid Nanofluid with Spherical NPs

Thermal Conductivity:

$$\frac{K_{TetraNF}}{K_{TriNF}}=\frac{\left(k_{S4}+2k_{TriNF}\right)-2\phi_4\left(k_{TriNF}-k_{S4}\right)}{\left(k_{S4}+2k_{TriNF}\right)+\phi_4\left(k_{TriNF}-k_{S4}\right)}$$

where

$$\frac{K_{TriNF}}{K_{hNF}}=\frac{\left(k_{S3}+2k_{hNFF}\right)-2\phi_3\left(k_{hNF}-k_{S3}\right)}{\left(k_{S3}+2k_{hNF}\right)+\phi_3\left(k_{hNF}-k_{S3}\right)},$$

$$\frac{K_{hNF}}{K_{NF}}=\frac{\left(k_{S2}+2k_{NF}\right)-2\phi_3\left(k_{hNF}-k_{S2}\right)}{\left(k_{S2}+2k_{NF}\right)+\phi_3\left(k_{NF}-k_{S2}\right)},$$

$$\frac{K_{NF}}{K_{BF}}=\frac{\left(k_{S1}+2k_{BF}\right)-2\phi_1\left(k_{BF}-k_{S1}\right)}{\left(k_{S1}+2k_{BF}\right)+\phi_1\left(k_{BF}-k_{S1}\right)}$$

Density:

$$\rho_{TetraNF}=\left(\rho_{BF}\right)\left[\left(1-\phi_{S1}\right)\left\{\left(1-\phi_{S2}\right)\left(1-\phi_{S3}\right)\left[\left(1-\phi_{S4}\right)+\phi_{S4}\left(\frac{\rho_{S4}}{\rho_{BF}}\right)\right]+\phi_{S3}\left(\frac{\rho_{S3}}{\rho_{BF}}\right)+\phi_{S2}\left(\frac{\rho_{S2}}{\rho_{BF}}\right)\right\}+\phi_{S1}\left(\frac{\rho_{S1}}{\rho_{BF}}\right)\right]$$

Specific Heat Capacity:

$$\left(\rho C_P\right)_{TetraNF}=\left(\rho C_{PBF}\right)\left(1-\phi_{S1}\right)\left[\left\{\left(1-\phi_{S2}\right)\left(1-\phi_{S3}\right)\left[\left(1-\phi_{S4}\right)+\phi_{S4}\left(\frac{\left(\rho C_P\right)_{S4}}{\left(\rho C_P\right)_{BF}}\right)\right]+\phi_{S3}\left(\frac{\left(\rho C_P\right)_{S3}}{\left(\rho C_P\right)_{BF}}\right)+\phi_{S2}\left(\frac{\left(\rho C_P\right)_{S2}}{\left(\rho C_P\right)_{BF}}\right)\right\}+\phi_{S1}\left(\frac{\left(\rho C_P\right)_{S1}}{\left(\rho C_P\right)_{BF}}\right)\right]$$

Viscosity:

$$\frac{\mu_{TetraNF}}{\mu_{BF}}=\frac{1}{\left(1-\phi_{S1}\right)^{2.5}\left(1-\phi_{S2}\right)^{2.5}\left(1-\phi_{S3}\right)^{2.5}\left(1-\phi_{S4}\right)^{2.5}}$$

Thermal expansion:

$$\beta_{TetraNF}=\left(\beta_{BF}\right)\left(1-\phi_{S1}\right)\left\{\left(1-\phi_{S2}\right)\left(1-\phi_{S3}\right)\left[\left(1-\phi_{S4}\right)+\phi_{S4}\left(\frac{\beta_{S4}}{\beta_{BF}}\right)\right]+\phi_{S3}\left(\frac{\beta_{S3}}{\beta_{BF}}\right)+\phi_{S2}\left(\frac{\beta_{S2}}{\beta_{BF}}\right)\right\}+\phi_{S1}\left(\frac{\beta_{S1}}{\beta_{BF}}\right)\Bigg]$$

According to [2], the temperature-dependent thermal conductivity and temperature-dependent viscosity of fluid are given, similarly, the temperature-dependent specific heat capacity and temperature density following [3] are written as:

$$\left.\begin{aligned}\mu_{Bf}\left(T^*\right)&=\mu_{Bf}\left(\mathrm{e}^{-a\left(\frac{T^*-T_\infty^*}{T_0^*-T_\infty^*}\right)}\right)\\ k_{Bf}\left(T^*\right)&=k_{Bf}\left(1-b\left(\frac{T^*-T_\infty^*}{T_0^*-T_\infty^*}\right)\right)\\ \rho_{Bf}\left(T^*\right)&=\rho_{Bf}\left[1+d\left(T^*-T_\infty^*\right)\right]\\ \left(\rho C_p\right)_{Bf}\left(T^*\right)&=\left(\rho C_p\right)_{Bf}\left[1+c\left(T^*-T_\infty^*\right)\right]\end{aligned}\right\} \tag{6}$$

Following [1] and [2] the temperature-dependent thermophysical properties of Tetra-PAO nanofluid can be written as follows:

$$\left.\begin{aligned}
\mu_{TetraNF}\left(T^*\right) &= \frac{\mu_{BF}\left(T^*\right)}{\left(1-\phi_{S1}\right)^{2.5}\left(1-\phi_{S2}\right)^{2.5}\left(1-\phi_{S3}\right)^{2.5}\left(1-\phi_{S4}\right)^{2.5}} \\
K_{TetraNF}\left(T^*\right) &= \frac{K_{TriNF}\left(T^*\right)\left(k_{S4}+2k_{TriNF}\right)-2\phi_4\left(k_{TriNF}-k_{S4}\right)}{\left(k_{S4}+2k_{TriNF}\right)+\phi_4\left(k_{TriNF}-k_{S4}\right)} \\
\left(\rho C_P\right)_{TetraNF}\left(T^*\right) &= \left(\rho C_{P\,BF}\right)\left(T^*\right)\left(1-\phi_{S1}\right)\left[\left\{\left(1-\phi_{S2}\right)\left(1-\phi_{S3}\right)\left[\left(1-\phi_{S4}\right)+\phi_{S4}\left(\frac{\left(\rho C_P\right)_{S4}}{\left(\rho C_P\right)_{BF}}\right)\right]\right.\right. \\
&\quad \left.\left.+\phi_{S3}\left(\frac{\left(\rho C_P\right)_{S3}}{\left(\rho C_P\right)_{BF}}\right)+\phi_{S2}\left(\frac{\left(\rho C_P\right)_{S2}}{\left(\rho C_P\right)_{BF}}\right)\right\}+\phi_{S1}\left(\frac{\left(\rho C_P\right)_{S1}}{\left(\rho C_P\right)_{BF}}\right)\right] \\
\rho_{TetraNF}\left(T^*\right) &= \left(\rho_{BF}\right)\left(T^*\right)\left[\left(1-\phi_{S1}\right)\left\{\left(1-\phi_{S2}\right)\left(1-\phi_{S3}\right)\left[\left(1-\phi_{S4}\right)+\phi_{S4}\left(\frac{\rho_{S4}}{\rho_{BF}}\right)\right]\right.\right. \\
&\quad \left.\left.+\phi_{S3}\left(\frac{\rho_{S3}}{\rho_{BF}}\right)+\phi_{S2}\left(\frac{\rho_{S2}}{\rho_{BF}}\right)\right\}+\phi_{S1}\left(\frac{\rho_{S1}}{\rho_{BF}}\right)\right]
\end{aligned}\right\} \tag{7}$$

Equation (6) into Equation (7) gives:

$$\left.\begin{aligned}
\mu_{TetraNF}\left(T^*\right) &= \frac{\mu_{BF}\left(\ell^{-\xi\theta\left(\eta^*\right)}\right)}{\left(1-\phi_{S1}\right)^{2.5}\left(1-\phi_{S2}\right)^{2.5}\left(1-\phi_{S3}\right)^{2.5}\left(1-\phi_{S4}\right)^{2.5}} \\
K_{TetraNF}\left(T^*\right) &= \frac{k_{TriNF}\left(k_{S3}+2k_{hNF}\right)-2\phi_3\left(k_{hNF}-k_{S3}\right)}{\left(k_{S3}+2k_{hNF}\right)+\phi_3\left(k_{hNF}-k_{S3}\right)}k_{BF}\left(1-\Omega\theta\left(\eta^*\right)\right) \\
\left(\rho C_P\right)_{TetraNF}\left(T^*\right) &= \left[\left(1-\phi_{S1}\right)\left\{\left(1-\phi_{S2}\right)\left(1-\phi_{S3}\right)\left[\left(1-\phi_{S4}\right)+\phi_{S4}\left(\frac{\left(\rho C_P\right)_{S4}}{\left(\rho C_P\right)_{BF}}\right)\right]+\phi_{S3}\left(\frac{\left(\rho C_P\right)_{S3}}{\left(\rho C_P\right)_{BF}}\right)\right.\right. \\
&\quad \left.\left.+\phi_{S2}\left(\frac{\left(\rho C_P\right)_{S2}}{\left(\rho C_P\right)_{BF}}\right)\right\}+\phi_{S1}\left(\frac{\left(\rho C_P\right)_{S1}}{\left(\rho C_P\right)_{BF}}\right)\left(\rho C_P\right)_{BF}\left(1+\varpi\theta\left(\eta^*\right)\right) \\
\rho_{TetraNF}\left(T^*\right) &= \left[\left(1-\phi_{S1}\right)\left\{\left(1-\phi_{S2}\right)\left(1-\phi_{S3}\right)\left[\left(1-\phi_{S4}\right)+\phi_{S4}\left(\frac{\rho_{S4}}{\rho_{BF}}\right)\right]\right.\right. \\
&\quad \left.\left.+\phi_{S3}\left(\frac{\rho_{S3}}{\rho_{BF}}\right)+\phi_{S2}\left(\frac{\left(\rho C_P\right)_{S2}}{\left(\rho C_P\right)_{BF}}\right)\right\}+\phi_{S1}\left(\frac{\rho_{S1}}{\rho_{BF}}\right)\right]\rho_{BF}\left(1+\alpha\theta\left(\eta^*\right)\right)
\end{aligned}\right\} \tag{8}$$

4. Similarity Performances

In this section, the similarity technique was used to transform the governing PDEs into ODEs. A similarity solution of the equation is usually obtained by defining an independent variable η^* and a dependent variable f in terms of the Stream function, Ψ^*.

The continuity Equation (1) is satisfied by defining the stream function:

$$\left.\begin{aligned}
\Psi^* &= \sqrt{\nu_{BF} x^* U_\infty^*}\, f\left(\eta^*\right) \\
\eta^* &= y^* \sqrt{\frac{U_\infty^*}{\nu_{BF} x^*}} \\
T^* &= \left(T_w^* - T_\infty^*\right)\theta\left(\eta^*\right) + T_\infty^* \\
u^* &= \frac{\partial \Psi^*}{\partial y^*} = U_\infty^* f'\left(\eta^*\right) \\
v^* &= -\frac{\partial \Psi^*}{\partial x^*} = -\frac{1}{2}\sqrt{\frac{U_\infty^* \nu_{BF}}{x^*}}\left(\eta^* f' - f\right)
\end{aligned}\right\} \tag{9}$$

After differentiating Equations (2)-(4) with Equation (5) by the quotient, product, and chain rules, the following equations were obtained:

$$\begin{aligned}
&\frac{\left(1+\alpha\theta\right)\ell^{-\zeta\theta} f''' - \left(\zeta \ell^{-\zeta\theta}\left(1+\alpha\theta\right) + \alpha\ell^{-\zeta\theta}\right) f''\theta'}{A^* B^* \left(1+\alpha\theta\right)^2} \\
&+\frac{1}{2} f f'' + C^* Gr_{T^*}\theta - \frac{\ell^{-\zeta\theta} K_*}{A^* B^* \left(1+\alpha\theta\right)} f' = 0
\end{aligned} \tag{10}$$

$$\begin{aligned}
&\frac{D^*}{E^*}\left[\frac{\left(\left(1+\varpi\theta\right)\left(1-\Omega\theta\right)\right)\theta'' - \left(\Omega\left(1+\varpi\theta\right) + \varpi\left(1-\Omega\theta\right)\right)\theta'^2}{\left(1+\varpi\theta\right)^2}\right] \\
&+\frac{1}{2}\overline{Pr} f\theta' + \frac{\overline{Br}\ell^{-\zeta\theta}}{B^* E^*\left(1+\varpi\theta\right)}\left(f''\right)^2 = 0
\end{aligned} \tag{11}$$

The boundary conditions are:

$$\begin{aligned}
f'(0) = 0,\ f(0) = S^*, \theta'(0) = -Bi\left(1-\theta(0)\right) \quad \text{at} \quad \eta^* = 0 \\
f'(\infty) \to 1, \theta(\infty) \to 0 \quad \text{as} \quad \eta^* \to \infty
\end{aligned} \tag{12}$$

where;

$$\begin{aligned}
A^* &= \left(1-\phi_{S1}\right)\left\{\left(1-\phi_{S2}\right)\left(1-\phi_{S3}\right)\left[\left(1-\phi_{S4}\right) + \phi_{S4}\left(\frac{\rho_{S4}}{\rho_{BF}}\right)\right]\right. \\
&\left. + \phi_{S3}\left(\frac{\rho_{S3}}{\rho_{BF}}\right) + \phi_{S2}\left(\frac{\rho_{S2}}{\rho_{BF}}\right)\right\} + \phi_{S1}\left(\frac{\rho_{S1}}{\rho_{BF}}\right) \\
B^* &= \left(1-\phi_{S1}\right)^{2.5}\left(1-\phi_{S2}\right)^{2.5}\left(1-\phi_{S3}\right)^{2.5}\left(1-\phi_{S4}\right)^{2.5} \\
C^* &= \left(1-\phi_{S1}\right)\left\{\left(1-\phi_{S2}\right)\left(1-\phi_{S3}\right)\left[\left(1-\phi_{S4}\right) + \phi_{S4}\left(\frac{\beta_{S4}}{\beta_{BF}}\right)\right]\right. \\
&\left. + \phi_{S3}\left(\frac{\beta_{S3}}{\beta_{BF}}\right) + \phi_{S2}\left(\frac{\beta_{S2}}{\beta_{BF}}\right)\right\} + \phi_{S1}\left(\frac{\beta_{S1}}{\beta_{BF}}\right) \\
D^* &= \frac{k_{TriNF}\left(k_{S4} + 2k_{TriNF}\right) - 2\phi_{S4}\left(k_{TriNF} - k_{S4}\right)}{\left(k_{S4} + 2k_{TriNF}\right) + \phi_{S4}\left(k_{TriNF} - k_{S4}\right)} \\
E^* &= \left(1-\phi_{S1}\right)\left\{\left(1-\phi_{S2}\right)\left(1-\phi_{S3}\right)\left[\left(1-\phi_{S4}\right) + \phi_{S4}\left(\frac{\left(\rho C_P\right)_{S4}}{\left(\rho C_P\right)_{BF}}\right)\right]\right. \\
&\left. + \phi_{S3}\left(\frac{\left(\rho C_P\right)_{S3}}{\left(\rho C_P\right)_{BF}}\right) + \phi_{S2}\left(\frac{\left(\rho C_P\right)_{S2}}{\left(\rho C_P\right)_{BF}}\right)\right\} + \phi_{S1}\left(\frac{\left(\rho C_P\right)_{S1}}{\left(\rho C_P\right)_{BF}}\right)
\end{aligned}$$

$\zeta = a\left(\frac{T_w^* - T_\infty^*}{T_0^* - T_\infty^*}\right)$ is variable viscosity, $\Omega = b\left(\frac{T_w^* - T_\infty^*}{T_0^* - T_\infty^*}\right)$ is the variable thermal conductivity, $\varpi = c\left(T_w^* - T_\infty^*\right)$ is the variable specific heat capacity, $\alpha = d\left(T_w^* - T_\infty^*\right)$ is the variable density, $\overline{Pr} = \frac{\mu_{BF} C_{PBF}}{k_{BF}}$ is Prandtl number, $\overline{Br} = \frac{\mu_{BF} U_\infty^{*2}}{k_{BF}\left(T_w^* - T_\infty^*\right)}$ is the Brinkmann number, $K_* = \frac{\mu_{BF} x^*}{\overline{k}\,\rho_{BF} U_\infty^*}$ is the permeability parameter, $Gr_{T^*} = \frac{\beta_{BF} g\left(T_w^* - T_\infty^*\right) x^*}{U_\infty^{*2}}$ is the Grashof number, $S^* = \frac{v_w^*}{2}\sqrt{\frac{U_\infty^* \upsilon_{BF}}{x^*}}$ is the suction, $Re = \frac{U_\infty^* x^*}{\upsilon_{BF}}$ is the Reynolds number, $Bi_* = \frac{h_w}{k}\sqrt{\frac{\upsilon_{BF} x^*}{U_\infty^*}}$ is the Biot number. The skin friction coefficient, ($\overline{C_f}$), and Nusselt number, ($\overline{Nu}$) are the imperative parameters which are defined as;

$$\overline{C_f} = \frac{\tau_w}{\rho_{BF} U_\infty^{*2}} \quad \text{and} \quad \overline{Nu} = \frac{x^* q_w}{k_{BF}\left(T_w^* - T_\infty^*\right)} \tag{13}$$

The shear stress, τ_w and wall heat flux, q_w are given as:

$$\tau_w = \mu_{TetraNF} \frac{\partial u^*}{\partial y^*} \quad \text{and} \quad q_w = -k_{TetraNF} \frac{\partial T^*}{\partial y^*} \tag{14}$$

$$\frac{\partial u^*}{\partial y^*} = \sqrt{\frac{U_\infty^{*3}}{\upsilon_{BF} x^*}} f''(0), \text{ and } \frac{\partial T^*}{\partial y^*} = \sqrt{\frac{U_\infty^*}{\upsilon_{BF} x^*}}\left(T_w^* - T_\infty^*\right)\theta'(0) \tag{15}$$

Substituting Equation (15) into Equation (14) and the resulting Equation into Equation (13) gives Equation (16)

$$\overline{C_f} = \frac{1}{\sqrt{Re}\left(1-\phi_1\right)^{2.5}\left(1-\phi_2\right)^{2.5}\left(1-\phi_3\right)^{2.5}\left(1-\phi_4\right)^{2.5}} f''(0), \text{ and } \overline{Nu} = -\frac{k_{TetraNF}}{k_{BF}}\sqrt{Re}\,\theta'(0) \tag{16}$$

where; $\frac{1}{\sqrt{Re}} = \sqrt{\frac{\upsilon_{BF}}{U_\infty^* x^*}}$.

5. Numerical Method

Equations (10) and (11) are coupled nonlinear third-order boundary value problems (BVPs), which cannot be easily solved analytically. Hence, the shooting technique is used to convert the governing BVPs into corresponding IVPs with specified initial value conditions. The unknown initial value conditions are guessed continuously until the boundary condition is satisfied in other to solve the IVPs.

The coupled nonlinear BVP ODEs, *i.e.* Equations (10) and (11) with the boundary conditions Equation (12) were reformed into the system of first-order ODEs as shown in the following:

$$\text{Let} \quad \begin{matrix} f = m_1, f' = m_1' = m_2, f'' = m_2' = m_3, f''' = m_3' = m_4, \\ \theta = m_5, \theta' = m_5' = m_6, \theta'' = m_6' = m_7 \end{matrix} \tag{17}$$

Putting Equation (17) into Equations (10)-(11) yields:

$$f''' = m_3' = m_4 = \left(\zeta\left(1+\alpha m_5\right)+\alpha\right)m_3 m_6 - \frac{A^* B^*\left(1+\alpha m_5\right)}{2\ell^{-\zeta m_5}} m_1 m_2 - \frac{A^* B^* C^* Gr_{T^*}\left(1+\alpha m_5\right)}{\ell^{-\zeta m_5}} m_5 + K_* m_2$$

$$\theta'' = m_6' = m_7 = \frac{\left[\Omega\left(1+\varpi m_5\right)+\varpi\left(1-\Omega m_5\right)\right]m_6^2}{\left(1+\varpi m_5\right)\left(1-\Omega m_5\right)} - \frac{E^*\left(1+\varpi m_5\right)\overline{Pr}}{2D^*\left(1-\Omega m_5\right)} m_1 m_6 - \frac{\overline{Br}\ell^{-\zeta m_5}}{B^* D^*\left(1-\Omega m_5\right)} m_3^2$$

subject to: $m_1(0) = S^*, m_2(0) = 0, m_3(0) = p, m_5(0) = q, m_6(0) = -Bi(1-q)$ (18)

where p and q are the unknown values of $f''(0)$ and $\theta(0)$ which are related to the wall shear stress and the temperature of the surface. These unknowns were chosen by guessing repeatedly until the boundary conditions $f'(\infty)\to 1$ and $\theta(\infty)\to 0$ were satisfied. Taking $\eta_\infty^* \approx 5$ arbitrarily, where $p = f'' = 0.350914274724478$ and $q = \theta(0) = 1.40636461202945$ were later gotten. The Runge-Kutta method of 4th order computations was done by substituting the values of the thermo-physical properties of TiO_2, SiO_2, ZnO, Fe_2O_3 and PAO with the aid of the Maple 18.0 software bundle.

6. Statistical Approach

Linear regression estimation analysis for Nusselt number as well as skin friction coefficient was done in this segment. The mathematical formula of linear regression was adopted from [20] as shown below. It describes the line of best fit for the relationship between $\vec{y}$ (dependent variable) and $\vec{x}$ (independent variable)

$$\vec{y} = b\vec{x} + a \tag{19}$$

where $a = \dfrac{\left(\sum \vec{y}\right)\left(\sum \vec{x}^2\right) - \left(\sum \vec{x}\right)\left(\sum \vec{x}\vec{y}\right)}{n\left(\sum \vec{x}^2\right) - \left(\sum \vec{x}\right)^2}$ is the intercept and

$b = \dfrac{n\left(\sum \vec{x}\vec{y}\right) - \left(\sum \vec{x}\right)\left(\sum \vec{y}\right)}{n\left(\sum \vec{x}^2\right) - \left(\sum \vec{x}\right)^2}$ is the slope of the line.

7. Results and Discussion

The thermophysical parameters of TiO_2-SiO_2-ZnO-Fe_2O_3/PAO tetra hybrid nanofluid taken into consideration here are suction, S^*, permeability parameter, K_*, Grashof number, Gr_{T^*}, Prandtl number, $\overline{Pr}$, Brinkmann number, $\overline{Br}$, Biot number, *Bi*, thermal conductivity constraint, Ω variable viscosity parameter, ζ, variable density parameter, α, and variable specific heat capacity parameter, ϖ. The exploration of their effects on the velocity and temperature profiles as

well as on the drag friction $f''(0)$ and the rate of heat transfer, $\theta'(0)$ was considered. The volume fraction of the four NPs is in the range $0 \le \phi \le 0.2$. Table 2 represents the values of the thermophysical properties of PAO and the four NPs.

Table 2. Thermo-physical properties of Polyalphaolefins, PAO and the four NPs [46].

Thermo-physical properties	Thermal conductivity k (W/mK)	Specific-heat Capacity C_p (J/kg·K)	Density ρ (kg/m^3)	Thermal expansion (per K)
Titanium oxide, (TiO_2)	8.9538	686.2	4250	8.5×10^{-6}
Silicon dioxide (SiO_2)	1.5	703	2200	5.6×10^{-7}
Zinc oxide (ZnO)	13	459.2	5600	4.77×10^{-5}
Iron oxide (Fe_2O_3)	80.4	670	5180	8.4×10^{-6}
Polyalphaolefins (PAO)	0.143	2303	798	3.5×10^{-4}

Comparison of this research with the work of [50] for the plate surface temperature $\theta(0)$ and the rate of heat transfer $-\theta'(0)$ varying Biot number, Bi showed that the values agree up to the fourth place of decimal as shown in Table 3.

Table 3. Comparison with [50] varying Biot number, Bi for $\overline{Br} = Gr_{T^*} = S^* = K_* = \zeta = \varpi = \Omega = \alpha = \phi = 0$, $\overline{Pr} = 0.72$.

	Ref. [50]	This study	Ref. [50]	This study
Bi	$\theta(0)$	$\theta(0)$	$-\theta'(0)$	$-\theta'(0)$
0.05	0.1447	0.14468	0.0428	0.04277
0.10	0.2528	0.25281	0.0747	0.07472
0.20	0.4035	0.40351	0.1193	0.11930
0.40	0.5750	0.57502	0.1700	0.16999
0.60	0.6699	0.66990	0.1981	0.19806
0.80	0.7302	0.730231	0.2159	0.21582
1.00	0.7718	0.771807	0.2282	0.22819

7.1. Numerical Results on the Velocity and Temperature Profiles

The influence of the considered thermophysical parameters on the skin friction and the Nusselt number at the outward of the plate are displayed in Tables 4-9.

Table 4 shows that as the variable thermal conductivity, Ω increases, the skin friction increases at the rate of **0.011697519**. Also, the increase in the Ω, makes the rate of heat transfer of the TiO_2-SiO_2-ZnO-Fe_2O_3/PAO Tetra hybrid nanofluid increased the rate of **8.043581616** which is so significant and in excellent agreement with the result of [50]. The observed increase in heat transfer rate with rising thermal conductivity underscores the potential for optimizing heat exchanger efficiency in various industrial applications.

Table 4. Impact variable thermal conductivity parameter, Ω on the skin friction, $f''(0)$ and Nusselt number $\theta'(0)$.

Variable thermal conductivity, Ω	$f''(0)$	$\theta'(0)$
0.03	0.351058776066758	4.16017800418291
0.05	0.351212157784214	4.26309162963490
0.10	0.351642224394989	4.55396319062010
0.20	0.352808472256885	5.35660041274862
0.25	0.353676054744617	5.96079246192667
Slope = rate of change	**0.011697519**	**8.043581616**

Table 5 reveals the influence of the variable viscosity parameter, ζ, on the skin friction and Nusselt number. As ζ rises the boundary layer of the surface intensifies leading to an increase of the drag friction at the rate of **0.476069294**. Similarly, the Nusselt number also increases at the rate of **1.163082775**. The influence of the variable viscosity parameter on both skin friction and Nusselt number highlights its role in boundary layer dynamics, indicating potential strategies for enhancing heat transfer efficiency in fluid systems.

Table 5. Impact variable viscosity parameter, ζ, on the skin friction coefficient, $f''(0)$ and Nusselt number $\theta'(0)$.

Variable viscosity, ζ	$f''(0)$	$\theta'(0)$
0.03	0.359072226643466	4.08850922132622
0.05	0.367441096293778	4.11316825576169
0.10	0.389321737261669	4.17378800545484
0.20	0.437489195987124	4.28954930533805
0.25	0.463957035163817	4.34407496120683
Slope = rate of change	**0.476069294**	**1.163082775**

Table 6. Impact variable density parameter, α on the skin friction, $f''(0)$ and Nusselt number $\theta'(0)$.

Variable density, α	$f''(0)$	$\theta'(0)$
0.03	0.359333767147346	4.26053631364450
0.05	0.367943213282502	4.46669660698397
0.10	0.390399616622081	5.02680003854599
0.20	0.440316840342745	6.38032550083036
0.25	0.468531670432957	7.20560818614124
Slope = rate of change	**0.494832**	**13.32044**

In **Table 6**, as variable density, α rises, both the skin friction and the Nusselt number increase at the rate of **0.494832** and **13.32044** respectively. These results

indicate greater momentum transfer and enhance convective heat transfer, respectively. This phenomenon is significant in industries like aerospace and thermal power generation, where optimizing fluid density variations improves heat transfer efficiency and system performance.

The skin friction of the surface declines as the variable specific heat capacity, ϖ increases at the rate of **−0.00871**, and the Nusselt number represented as $\theta'(0)$ also decreases as ϖ at the rate of **−2.50981** in Table 7. This signifies reduced surface friction and convective heat transfer rates. This has practical implications in industries like thermal engineering and aerospace, where optimizing specific heat capacity variations improves system performance and efficiency.

Table 7. Impact variable specific heat capacity parameter, ϖ on the skin friction, $f''(0)$ and Nusselt number.

Variable specific heat capacity, ϖ	$f''(0)$	$\theta'(0)$
0.03	0.350670323204245	3.98986366311828
0.05	0.350442979279876	3.92185913613599
0.10	0.349933959818511	3.77214928355099
0.20	0.349099711652642	3.53378798681079
0.25	0.348747860939113	3.43552900302350
Slope = rate of change	**−0.00871**	**−2.50981**

Influence of suction parameter, $S^{\cdot}$ is shown in Table 8. As the suction parameter rises, the skin friction coefficient $f''(0)$ increases but the Nusselt number, $\theta'(0)$ decreases at the rate of **0.36583** and **−11.2527** respectively. This can be attributed to the stronger flow towards the surface, leading to increased shear stress and reduced residence time for convective heat transfer. These results are crucial for enhancing system performance in applications like high-speed vehicle cooling systems and heat exchanger design.

Table 8. Impact Suction parameter, $S^{\cdot}$ on the skin friction coefficient, $f''(0)$ and Nusselt number $\theta'(0)$.

Suction, $S^{\cdot}$	$f''(0)$	$\theta'(0)$
0.03	0.357819612576195	4.14844148977941
0.05	0.364724333829539	4.11117569509661
0.10	0.382260153968042	3.67581590991200
0.20	0.419106332804941	2.37907293307899
0.25	0.438345260564972	1.76832303332010
Slope = rate of change	**0.36583**	**−11.2527**

Table 9 shows that as the permeability parameter, $K_{\cdot}$ increases, both the skin friction coefficient and Nusselt number decrease at the rate of **−3.04929** and **−36.5618** respectively. Increasing permeability parameters in porous media

reduces flow resistance which leads to enhancing fluid movement, and heat transfer efficiency due to easier flow paths for the fluid, resulting in decreased skin friction and increased convective heat transfer.

Table 9. Impact of permeability parameter, K_* on the skin friction, $f''(0)$ and Nusselt number $\theta'(0)$.

Permeability parameter, K_*	$f''(0)$	$\theta'(0)$
0.02	0.322384401278756	3.53377502395164
0.03	0.293347465509687	3.02743490907725
0.04	0.263763079881543	2.54739284219257
0.06	0.233589257753860	2.09709600336063
0.1	0.0728610655102404	0.496352527920766
Slope = rate of change	**−3.04929**	**−36.5618**

7.2. Graphical Presentation of Results on the Velocity and Temperature Profiles

7.2.1. Impact of Thermophysical Parameters on the Velocity Profile

In this section, the thermophysical parameters considered are $\Omega = 0.01$, $\alpha = 0.01$, $\varpi = 0.01$, $\phi = 0.01$, $K_* = 0.01$, $S^* = 0.01$, $Gr_{T^*} = 0.01$, $\overline{Pr} = 120$, $\overline{Br} = 100$, $Bi = 10$. **Figures 2-5** show the influence of thermophysical parameters on the velocity profile. **Figure 2**, **Figure 3** and **Figure 5** illustrate that the velocity profiles increase as the variable viscosity, ζ, variable density parameter, α, and suction parameter, S^*, increase. The work of viscosity is to increase the drag force. However, the presence of buoyancy force increases the rate of movement of TiO_2-SiO_2-ZnO-Fe_2O_3/PAO tetra hybrid nanofluid. Suction filters dirt from the

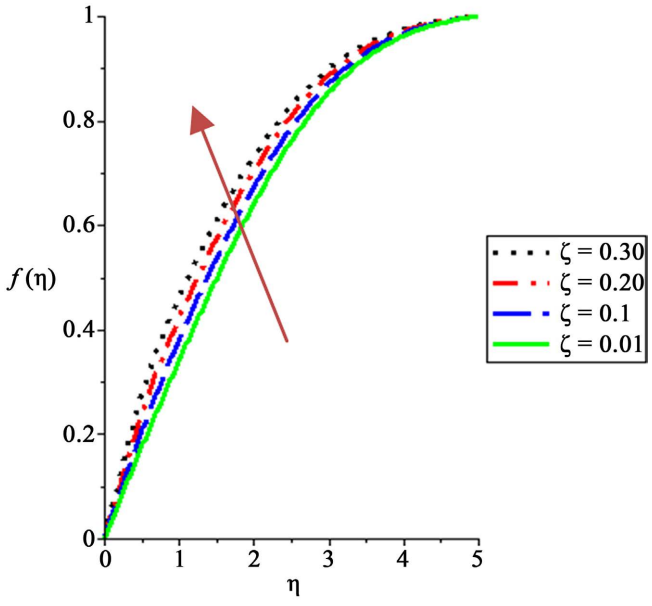

Figure 2. Velocity profile varying, ζ.

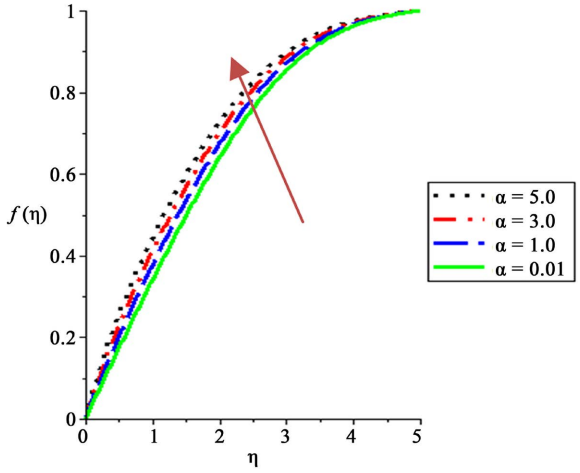

Figure 3. Velocity profile varying α.

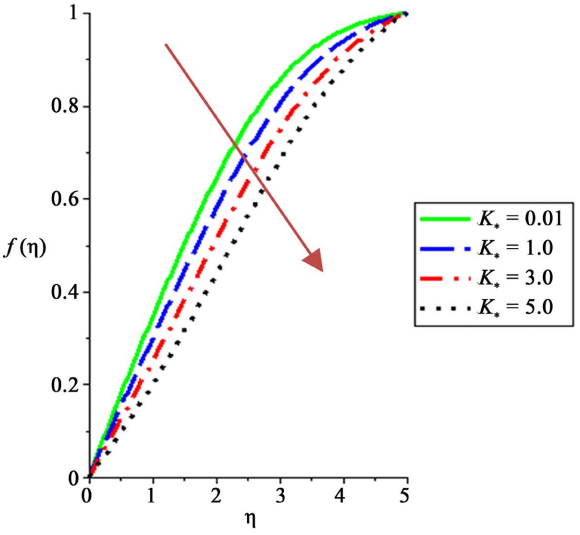

Figure 4. Velocity profile varying K_*.

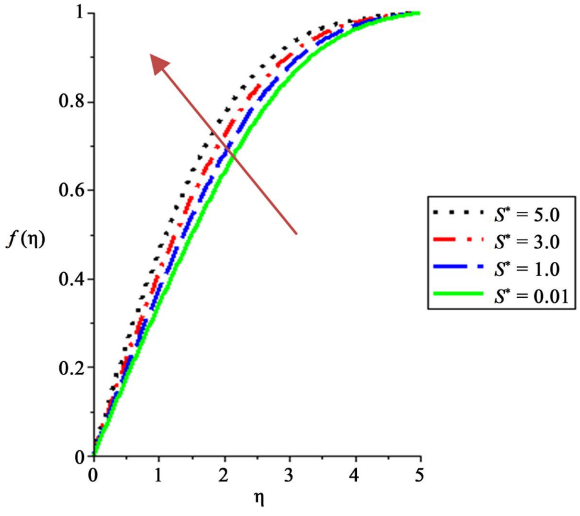

Figure 5. Velocity profile varying S^*.

TiO_2-SiO_2-ZnO-Fe_2O_3/PAO tetra hybrid nanofluid by this means alleviates the boundary layer and enhances the velocity profile. Conversely, due to sucking viscous TiO_2-SiO_2-ZnO-Fe_2O_3/PAO tetra hybrid nanofluid, as a permeability parameter, K, rises, the velocity profile declines which was displayed in Figure 4.

7.2.2. Impact of Thermophysical Parameters on the Temperature Profile

Figures 6-12 represent the effect of thermophysical properties on the temperature profile. Figure 6 and Figure 12 reveal that the temperature profile escalates

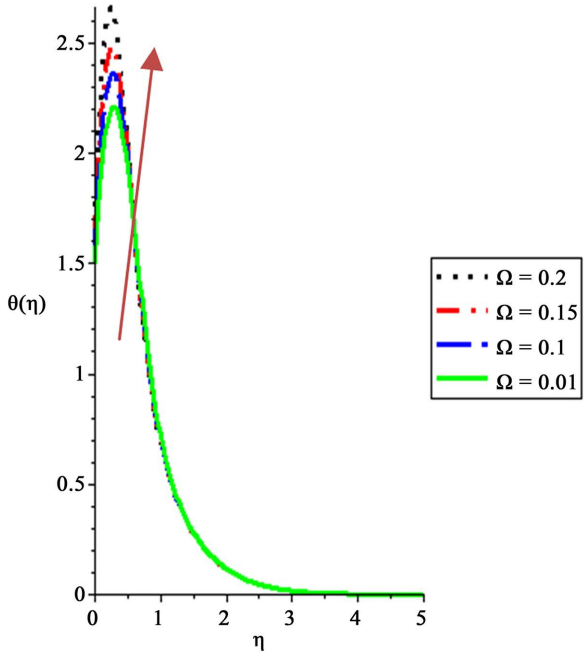

Figure 6. Temperature profile varying, Ω.

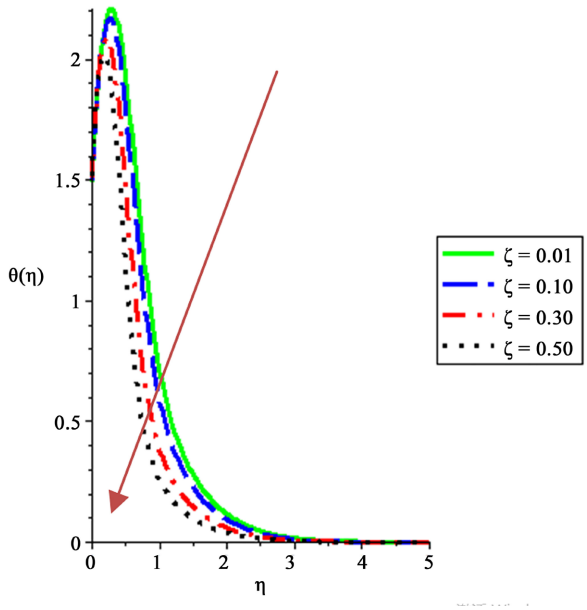

Figure 7. Temperature profile varying, ζ.

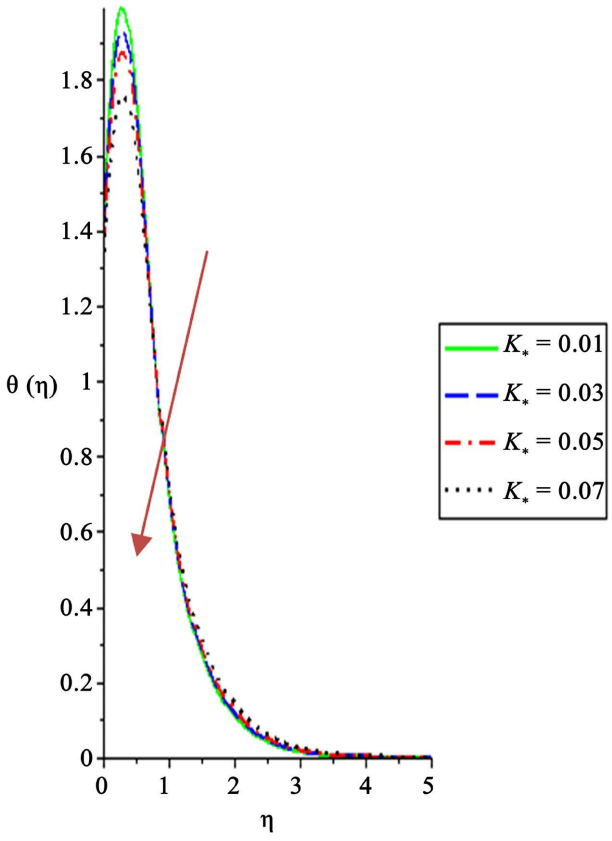

Figure 8. Temperature profile varying K_*.

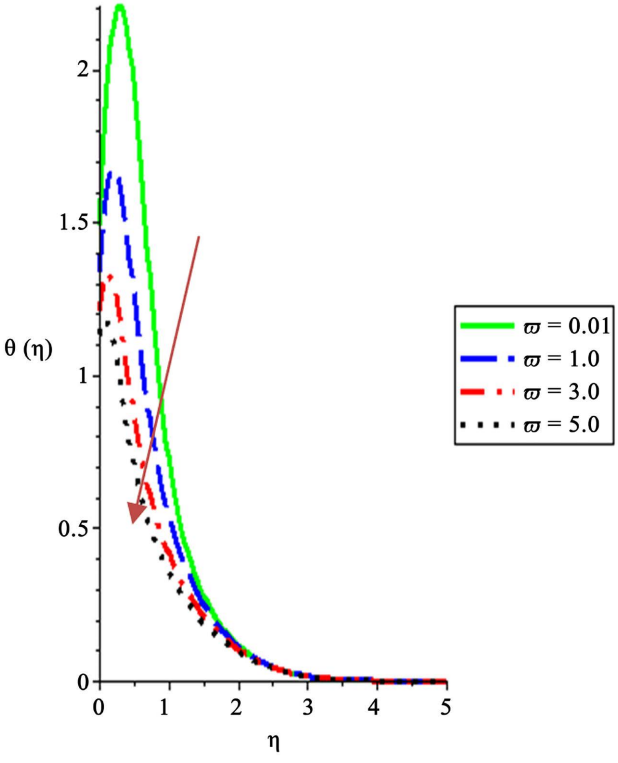

Figure 9. Temperature profile varying ϖ.

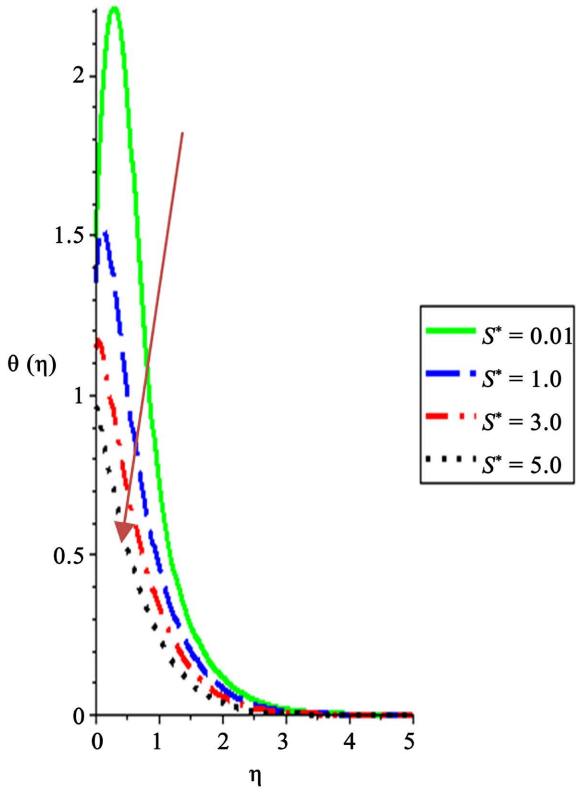

Figure 10. Temperature profile varying S^*.

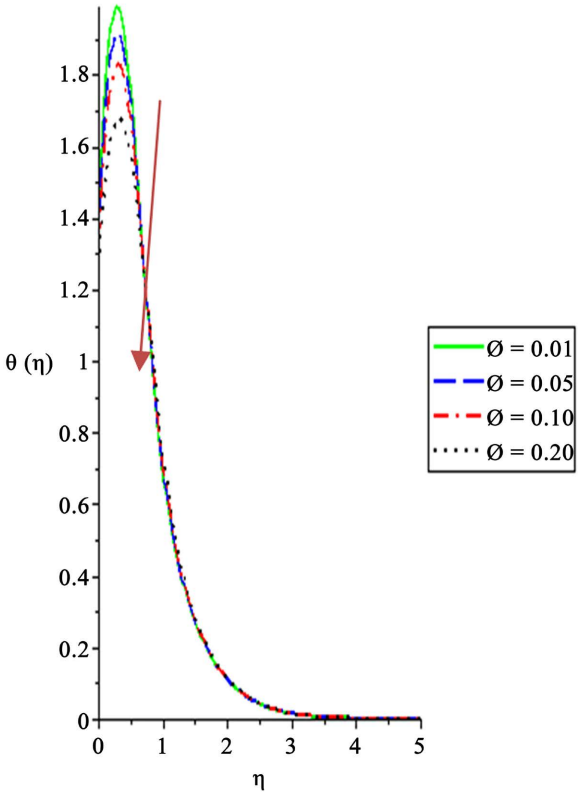

Figure 11. Temperature profile varying ϕ.

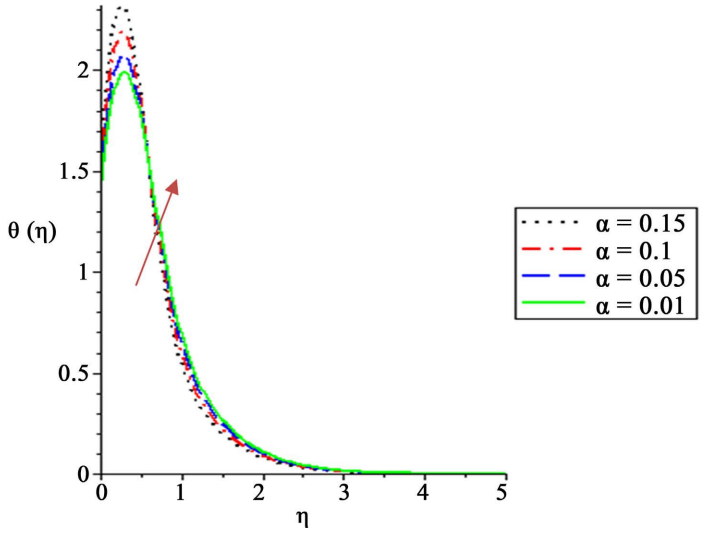

Figure 12. Temperature profile varying *a*.

as thermal conductivity, Ω and variable density parameters increase respectively. TiO_2-SiO_2-ZnO-Fe_2O_3/PAO tetra hybrid nanofluid absorbs more heat leading to an increase in the temperature of the fluid. **Figures 7-11** show that the temperature profiles decline as variable viscosity parameter, ζ, permeability parameter, K_*, variable specific heat capacity parameter, ϖ, suction, S^*, and volume fraction ϕ respectively, as viscosity is inversely proportional to temperature. Following the definition of specific heat capacity which is the quantity of heat required to cause a unit of mass (gram or kilogram) to change its temperature. $Q = mC_p\Delta T$, where C_p is the specific heat capacity and it is inversely proportional to temperature, which means that as specific heat capacity increases, the temperature decreases.

8. Conclusions

The numerical and statistical techniques were explored to investigate the influence of the combined temperature thermophysical properties on the dissipative movement of TiO_2-SiO_2-ZnO-Fe_2O_3/PAO tetra hybrid nanofluid in the presence of suction along a vertical porous surface. The study demonstrates that the thermophysical properties of TiO_2-SiO_2-ZnO-Fe_2O_3/PAO tetra hybrid nanofluid are crucial in the enhancement of the rate of heat transfer in the system.

1) An increase in the variable thermal conductivity of TiO_2-SiO_2-ZnO-Fe_2O_3/PAO tetra hybrid nanofluid increases the skin friction, Nusselt number, and temperature profile.

2) The skin friction and the Nusselt number increase as the variable viscosity increases, whereas the temperature profiles decrease.

3) As the variable density increases, the velocity profile increases, similarly, both the skin friction and Nusselt number increase.

4) An increase in the variable specific heat capacity increases the temperature profile and both the skin friction coefficient and Nusselt number.

Compared to previous literature, this research provides deeper insights into Tetra hybrid nanofluid behaviour, offering substantial advancements for heat transfer optimization. Future research avenues may explore broader parameter variations, experimental validation, and applications in diverse industrial contexts, further enhancing the field's understanding and practical implementation. It can also be concluded that linear regression is an excellent approach to give more insights into the relationship between the dependent variables and the independent variables of the boundary layer flow of TiO_2-SiO_2-ZnO-Fe_2O_3/PAO tetra hybrid nanofluid.

Conflicts of Interest

The authors declare no conflicts of interest regarding the publication of this paper.

References

[1] Sajid, T., Gari, A.A., Jamshed, W., Eid, M.R., Islam, N., Irshad, K., *et al.* (2023) Case Study of Autocatalysis Reactions on Tetra Hybrid Binary Nanofluid Flow *via* Riga Wedge: Biofuel Thermal Application. *Case Studies in Thermal Engineering*, **47**, Article ID: 103058. https://doi.org/10.1016/j.csite.2023.103058

[2] Khan, D., Kumam, P., Watthayu, W. and Jarad, F. (2024) Exploring the Potential of Heat Transfer and Entropy Generation of Generalized Dusty Tetra Hybrid Nanofluid in a Microchannel. *Chinese Journal of Physics*, **89**, 1009-1023. https://doi.org/10.1016/j.cjph.2023.10.006

[3] Zhao, J., Tian, S., Xie, H. and Zhang, X. (2023) Study of Time-Varying Laws of Stability and Wettability of SiO_2-H_2O Nanofluids with Different Particle Sizes. *Industrial & Engineering Chemistry Research*, **62**, 13529-13540. https://doi.org/10.1021/acs.iecr.3c02110

[4] Rashidi, M.M., Alhuyi Nazari, M., Mahariq, I. and Ali, N. (2022) Modeling and Sensitivity Analysis of Thermal Conductivity of Ethylene Glycol-Water Based Nanofluids with Alumina Nanoparticles. *Experimental Techniques*, **47**, 83-90. https://doi.org/10.1007/s40799-022-00567-4

[5] Wang, X., Song, Y., Li, C., Zhang, Y., Ali, H.M., Sharma, S., Li, R., Yang, M., Gao, T., Liu, M. and Cui, X. (2023). Nanofluids Application in Machining: A Comprehensive Review. *The International Journal of Advanced Manufacturing Technology*, **131**, 3113-3164.

[6] Ajeeb, W., Thieleke da Silva, R.R.S. and Murshed, S.M.S. (2023) Experimental Investigation of Heat Transfer Performance of Al_2O_3 Nanofluids in a Compact Plate Heat Exchanger. *Applied Thermal Engineering*, **218**, Article ID: 119321. https://doi.org/10.1016/j.applthermaleng.2022.119321

[7] Younes, H., Mao, M., Sohel Murshed, S.M., Lou, D., Hong, H. and Peterson, G.P. (2022) Nanofluids: Key Parameters to Enhance Thermal Conductivity and Its Applications. *Applied Thermal Engineering*, **207**, Article ID: 118202. https://doi.org/10.1016/j.applthermaleng.2022.118202

[8] Tawfik, M.M. (2017) Experimental Studies of Nanofluid Thermal Conductivity Enhancement and Applications: A Review. *Renewable and Sustainable Energy Reviews*, **75**, 1239-1253. https://doi.org/10.1016/j.rser.2016.11.111

[9] Yasmin, H., Giwa, S.O., Noor, S. and Sharifpur, M. (2023) Thermal Conductivity

Enhancement of Metal Oxide Nanofluids: A Critical Review. *Nanomaterials*, **13**, Article 597. https://doi.org/10.3390/nano13030597

[10] Pavía, M., Alajami, K., Estellé, P., Desforges, A. and Vigolo, B. (2021) A Critical Review on Thermal Conductivity Enhancement of Graphene-Based Nanofluids. *Advances in Colloid and Interface Science*, **294**, Article ID: 102452. https://doi.org/10.1016/j.cis.2021.102452

[11] Iqbal, M., Kouloulias, K., Sergis, A. and Hardalupas, Y. (2023) Critical Analysis of Thermal Conductivity Enhancement of Alumina-Water Nanofluids. *Journal of Thermal Analysis and Calorimetry*, **148**, 9361-9389. https://doi.org/10.1007/s10973-023-12334-7

[12] Zhang, Y. and Xu, X. (2020) Predicting the Thermal Conductivity Enhancement of Nanofluids Using Computational Intelligence. *Physics Letters A*, **384**, Article ID: 126500. https://doi.org/10.1016/j.physleta.2020.126500

[13] Ahmadi, M.H., Mirlohi, A., Alhuyi Nazari, M. and Ghasempour, R. (2018) A Review of Thermal Conductivity of Various Nanofluids. *Journal of Molecular Liquids*, **265**, 181-188. https://doi.org/10.1016/j.molliq.2018.05.124

[14] Zhou, L., Zhu, J., Zhao, Y. and Ma, H. (2022) A Molecular Dynamics Study on Thermal Conductivity Enhancement Mechanism of Nanofluids—Effect of Nanoparticle Aggregation. *International Journal of Heat and Mass Transfer*, **183**, Article ID: 122124. https://doi.org/10.1016/j.ijheatmasstransfer.2021.122124

[15] Manjunatha, S., Ammani Kuttan, B., Jayanthi, S., Chamkha, A. and Gireesha, B.J. (2019) Heat Transfer Enhancement in the Boundary Layer Flow of Hybrid Nanofluids Due to Variable Viscosity and Natural Convection. *Heliyon*, **5**, e01469. https://doi.org/10.1016/j.heliyon.2019.e01469

[16] Patra, A.K., Nayak, M.K. and Misra, A. (2020) Viscosity of Nanofluids—A Review. *International Journal of Thermofluid Science and Technology*, **7**, Article No. 070202. https://doi.org/10.36963/ijtst.2020070202

[17] Murshed, S.M.S. and Estellé, P. (2017) A State of the Art Review on Viscosity of Nanofluids. *Renewable and Sustainable Energy Reviews*, **76**, 1134-1152. https://doi.org/10.1016/j.rser.2017.03.113

[18] Ajala, O.A., Aselebe, L.O. and Ogunwobi, A. (2016) Boundary Layer Flow and Heat Transfer with Variable Viscosity in the Presence of Magnetic Field. *Journal of Advances in Mathematics*, **12**, 6412-6421. https://doi.org/10.24297/jam.v12i7.3874

[19] Ajala, O.A., Aselebe, L.O., Abimbade, S.F. and Ogunsola, A.W. (2019) Effect of Magnetic Fields on the Boundary Layer Flow of Heat Transfer with Variable Viscosity in the Presence of Thermal Radiation. *International Journal of Scientific and Research Publications* (*IJSRP*), **9**, 13-19. https://doi.org/10.29322/ijsrp.9.05.2019.p8904

[20] Lee, K.C., bin Saipolbahri, Z.A., Soleimani, H., Zaid, H.M., Guan, B.H. and Chuan Ching, D.L. (2016) Effect of Zinc Oxide Nanoparticle Sizes on Viscosity of Nanofluid for Application in Enhanced Oil Recovery. *Journal of Nano Research*, **38**, 36-39. https://doi.org/10.4028/www.scientific.net/jnanor.38.36

[21] Nabil, M.F., Azmi, W.H., Abdul Hamid, K., Mamat, R. and Hagos, F.Y. (2017) An Experimental Study on the Thermal Conductivity and Dynamic Viscosity of TiO_2-SiO_2 Nanofluids in Water: Ethylene Glycol Mixture. *International Communications in Heat and Mass Transfer*, **86**, 181-189. https://doi.org/10.1016/j.icheatmasstransfer.2017.05.024

[22] Azmi, W.H., Sharma, K.V., Mamat, R., Najafi, G. and Mohamad, M.S. (2016) The Enhancement of Effective Thermal Conductivity and Effective Dynamic Viscosity of

Nanofluids—A Review. *Renewable and Sustainable Energy Reviews*, **53**, 1046-1058. https://doi.org/10.1016/j.rser.2015.09.081

[23] Selvakumar, R.D. and Wu, J. (2019) A Comprehensive Model for Effective Density of Nanofluids Based on Particle Clustering and Interfacial Layer Formation. *Journal of Molecular Liquids*, **292**, Article ID: 111415. https://doi.org/10.1016/j.molliq.2019.111415

[24] Hu, Y., Li, Y., Lu, L., Mao, Y. and Li, M. (2020) Natural Convection of Water-Based Nanofluids near the Density Maximum in an Annulus. *International Journal of Thermal Sciences*, **152**, Article ID: 106309. https://doi.org/10.1016/j.ijthermalsci.2020.106309

[25] Ramprasad, T. and Suresh, A.K. (2023) Absorption of Co_2 in Nanofluids: Influence of the Material Density of Nanoparticles and a Correlating Principle. *Industrial & Engineering Chemistry Research*, **62**, 19205-19215. https://doi.org/10.1021/acs.iecr.3c00667

[26] Chavan, D. and Pise, A. (2019) Experimental Investigation of Effective Viscosity and Density of Nanofluids. *Materials Today*: *Proceedings*, **16**, 504-515. https://doi.org/10.1016/j.matpr.2019.05.122

[27] Mondragón, R., Juliá, J.E., Cabedo, L. and Navarrete, N. (2018) On the Relationship between the Specific Heat Enhancement of Salt-Based Nanofluids and the Ionic Exchange Capacity of Nanoparticles. *Scientific Reports*, **8**, Article No. 7532. https://doi.org/10.1038/s41598-018-25945-0

[28] Adun, H., Wole-Osho, I., Okonkwo, E.C., Kavaz, D. and Dagbasi, M. (2021) A Critical Review of Specific Heat Capacity of Hybrid Nanofluids for Thermal Energy Applications. *Journal of Molecular Liquids*, **340**, Article ID: 116890. https://doi.org/10.1016/j.molliq.2021.116890

[29] Sang, L. and Liu, T. (2017) The Enhanced Specific Heat Capacity of Ternary Carbonates Nanofluids with Different Nanoparticles. *Solar Energy Materials and Solar Cells*, **169**, 297-303. https://doi.org/10.1016/j.solmat.2017.05.032

[30] Chu, Y., Bashir, S., Ramzan, M. and Malik, M.Y. (2022) Model-Based Comparative Study of Magnetohydrodynamics Unsteady Hybrid Nanofluid Flow between Two Infinite Parallel Plates with Particle Shape Effects. *Mathematical Methods in the Applied Sciences*, **46**, 11568-11582. https://doi.org/10.1002/mma.8234

[31] Mahmood, Z., Eldin, S.M., Rafique, K. and Khan, U. (2023) Numerical Analysis of MHD Tri-Hybrid Nanofluid over a Nonlinear Stretching/Shrinking Sheet with Heat Generation/absorption and Slip Conditions. *Alexandria Engineering Journal*, **76**, 799-819. https://doi.org/10.1016/j.aej.2023.06.081

[32] Babar, H., Sajid, M. and Ali, H. (2019) Viscosity of Hybrid Nanofluids: A Critical Review. *Thermal Science*, **23**, 1713-1754. https://doi.org/10.2298/tsci181128015b

[33] Paul, A. and Patgiri, B. (2024) Modelling of Silicone Oil–based Casson Hybrid Nanofluid across a Porous Rotating Disk. In: Gupta, R. and Awasthi, M.K., Eds., *Modeling and Simulation of Fluid Flow and Heat Transfer*, CRC Press, 162-179. https://doi.org/10.1201/9781032712079-11

[34] Saeed, A., Alghamdi, W., Mukhtar, S., Shah, S.I.A., Kumam, P., Gul, T., *et al.* (2021) Darcy-Forchheimer Hybrid Nanofluid Flow over a Stretching Curved Surface with Heat and Mass Transfer. *PLOS ONE*, **16**, e0249434. https://doi.org/10.1371/journal.pone.0249434

[35] Aghakhani, S., Hajatzadeh Pordanjani, A., Afrand, M., Farsani, A.K., Karimi, N. and Sharifpur, M. (2023) Entropy Generation and Exergy Analysis of Ag-MgO/water Hybrid Nanofluid within a Circular Heatsink with Different Number of Outputs.

International Journal of Thermal Sciences, **184**, Article ID: 107891. https://doi.org/10.1016/j.ijthermalsci.2022.107891

[36] Jeelani, M.B. and Abbas, A. (2023) Al_2O_3-Cu\Ethylene Glycol-Based Magnetohydrodynamic Non-Newtonian Maxwell Hybrid Nanofluid Flow with Suction Effects in a Porous Space: Energy Saving by Solar Radiation. *Symmetry*, **15**, Article 1794. https://doi.org/10.3390/sym15091794

[37] Nanda, P., Sandeep, N., Sulochana, C. and Ashwinkumar, G.P. (2023) Enhanced Heat Transmission in Methanol-Based AA7072/AA7075 Tangent Hyperbolic Hybrid Nanofluid Flow along a Nonlinear Expandable Surface. *Numerical Heat Transfer*, *Part A*: *Applications*, **83**, 711-725. https://doi.org/10.1080/10407782.2022.2157916

[38] Hussain, S.M., Mahat, R., Katbar, N.M., Ullah, I., Varun Kumar, R.S., Prasannakumara, B.C., *et al.* (2023) Artificial Neural Network Modeling of Mixed Convection Viscoelastic Hybrid Nanofluid across a Circular Cylinder with Radiation Effect: Case Study. *Case Studies in Thermal Engineering*, **50**, Article ID: 103487. https://doi.org/10.1016/j.csite.2023.103487

[39] Ahmad, S., Ali, K., Ayub, A., Bashir, U., Rashid, F.L., Aryanfar, Y., *et al.* (2023) Localized Magnetic Fields and Their Effects on Heat Transfer Enhancement and Vortices Generation in Tri-Hybrid Nanofluids: A Novel Investigation. *Case Studies in Thermal Engineering*, **50**, Article ID: 103408. https://doi.org/10.1016/j.csite.2023.103408

[40] Adnan, Abbas, W., Bani-Fwaz, M.Z. and Kenneth Asogwa, K. (2023) Thermal Efficiency of Radiated Tetra-Hybrid Nanofluid $[(Al_2O_3\text{-}CuO\text{-}TiO_2\text{-}Ag)/Water]_{tetra}$ under Permeability Effects over Vertically Aligned Cylinder Subject to Magnetic Field and Combined Convection. *Science Progress*, **106**, 1-17. https://doi.org/10.1177/00368504221149797

[41] Paul, A., Patgiri, B. and Sarma, N. (2024) Darcy-forchheimer Flow of Ag-ZnO-$CoFe_2O_4/H_2O$ Casson Ternary Hybrid Nanofluid Induced by a Rotatory Disk with EMHD. *International Journal of Ambient Energy*, **45**, Article ID: 2313697. https://doi.org/10.1080/01430750.2024.2313697

[42] Paul, A., Patgiri, B. and Sarma, N. (2024) Transformer Oil-based Casson Ternary Hybrid Nanofluid Flow Configured by a Porous Rotating Disk with Hall Current. *ZAMM—Journal of Applied Mathematics and Mechanics/Zeitschrift für Angewandte Mathematik und Mechanik*, **104**, e202300704. https://doi.org/10.1002/zamm.202300704

[43] Khan, D., Hussien, M.A., Elsiddieg, A.M.A., Lone, S.A. and Hassan, A.M. (2023) Exploration of Generalized Two-Phase Free Convection Magnetohydrodynamic Flow of Dusty Tetra-Hybrid Casson Nanofluid between Parallel Microplates. *Nanotechnology Reviews*, **12**, Article ID: 20230102. https://doi.org/10.1515/ntrev-2023-0102

[44] Patgiri, B. and Paul, A. (2024) Inspection of Viscoelastic Ag + Cu + Fe_3O_4 + Al_2O_3/Kerosene Oil Tetra-Hybrid Nanofluid Flow across a Stretchable Rotating Disk with Exponentially Varying Viscosity. *Journal of Taibah University for Science*, **18**, Article ID: 2336327.

[45] Thanh, N.V., Ngoc, N.T.H., Thuy, D.M., Tuynh, L.V., Son, H.H. and Long, N.P. (2023) Highly Improved Dielectric and Thermal Performance of Polyalphaolefin Oil-Based Fluids Using MgO Nanoparticles. *Coatings*, **13**, Article 931. https://doi.org/10.3390/coatings13050931

[46] Makinde, O.D. and Makinde, A.E. (2023) Thermal Analysis of a Reactive Variable Viscosity TiO_2-PAO Nanolubricant in a Microchannel Poiseuille Flow. *Micromachines*, **14**, Article 1164. https://doi.org/10.3390/mi14061164

[47] Goharzadeh, A., Fatt, Y.Y. and Sangwai, J.S. (2023) Effect of TiO_2-SiO_2 Hybrid Nanofluids on Enhanced Oil Recovery Process under Different Wettability Conditions. *Capillarity*, **8**, 1-10. https://doi.org/10.46690/capi.2023.07.01

[48] Zhou, K., Ding, Y., Zhang, L., Wu, H. and Guo, J. (2020) Synthesis of Mesoporous ZnO/TiO_2-SiO_2 Composite Material and Its Application in Photocatalytic Adsorption Desulfurization without the Addition of an Extra Oxidant. *Dalton Transactions*, **49**, 1600-1612. https://doi.org/10.1039/c9dt04454j

[49] Borode, A., Tshephe, T., Olubambi, P., Sharifpur, M. and Meyer, J. (2023) Stability and Thermophysical Properties of GNP-Fe_2O_3 Hybrid Nanofluid: Effect of Volume Fraction and Temperature. *Nanomaterials*, **13**, Article 1238. https://doi.org/10.3390/nano13071238

[50] Etwire, C.J., Seini, I.Y., Musah, R. and Makinde, O.D. (2018) Combined Effects of Variable Viscosity and Thermal Conductivity on Dissipative Flow of Oil-Based Nanofluid over a Permeable Vertical Surface. *Diffusion Foundations*, **16**, 158-176. https://doi.org/10.4028/www.scientific.net/df.16.158

Nomenclature

Parameter	*Meaning*
u^*, v^*	Velocity components
x^*, y^*	Dimensional components
T^*	Temperature
U_∞^*	Stream velocity
g	Gravitational acceleration
$\mu_{TetraNF}\left(T^*\right)$	Temperature-dependent viscosity of tetra-PAO nanofluid
$K_{TetraNF}\left(T^*\right)$	Temperature-dependent Thermal conductivity of tetra-PAO nanofluid
$\left(\rho C_P\right)_{TetraNF}\left(T^*\right)$	Temperature-dependent Specific heat capacity of tetra-PAO nanofluid
$\rho_{TetraNF}\left(T^*\right)$	Temperature-dependent Density of tetra-PAO nanofluid
μ_{BF}	Viscosity of base fluid
K_{BF}	Thermal conductivity of the base fluid
$\left(\rho C_P\right)_{BF}$	Specific heat capacity of the base fluid
ρ_{BF}	Density of the base fluid